Reheat Response and Accelerated Cooling of a Microalloyed Steel with an Air/Water Atomizer: Effect on Microstructure and Mechanical Properties

S.R. Pejavar and P.B. Aswath

The use of an atomizer for accelerated cooling is discussed. An atomizer is an effective tool for controlling the microstructure and properties of a microalloyed steel because of its flexibility of operation and control of cooling rate over a broad range of temperatures. Some basic issues regarding heat transfer in pool boiling and in spray cooling also are presented. Reheating response studies were conducted in addition to studies of the effect of accelerated cooling on the microstructure and properties of a low-carbon steel microalloyed with niobium and vanadium. This steel produces a tempered martensitic microstructure on quenching and a predominantly bainitic microstructure at slower cooling rates. The yield, tensile, and fracture strengths can be tailored by controlling the cooling rate, which in turn can be controlled by the air/water ratio and flow rates in the atomizer. Impact toughness is a function of cooling rate and reaches a maximum followed by a decrease, probably due to the formation of upper bainite at lower cooling rates. Fractographic studies indicated that tensile fracture occurred by microvoid coalescence, with the dimple size decreasing as the cooling rate decreased. Charpy impact fracture studies indicated that the primary mode of failure was by quasi-cleavage, with the number of secondary cracks also decreasing as the cooling rate decreased.

Keywords

accelerated cooling, atomizer, bainite, heat transfer, HSLA steels (high strength low alloy), tempered martensite

1. Introduction

HIGH-STRENGTH low-alloy (HSLA) steels are examples of an efficient metallurgical innovation in which alloying addition and thermomechanical processing have been brought together to obtain improved engineering properties through microstructural control. The practice is inexpensive because of the small concentration of alloying additions and because the thermomechanical processing is simply a modification of the final hot-forming operation.

The relationships among composition, microstructure, and mechanical properties of HSLA steels have been extensively studied (Ref 1). The metallurgical characteristics that affect the microstructure/mechanical property relationships exhibited by these steels include (Ref 1):

- The size and shape of grains of the final transformation product
- Precipitate size and volume fraction
- Dislocation density
- Nonmetallic inclusion volume fraction and shape

Most HSLA steels currently used are quenched and tempered. This provides good strength levels, but also presents several major drawbacks, including the need for an expensive quenching plant, and limitations on product size and shape, an extra tempering treatment step, and increased alloying content to achieve the required hardenability.

For these reasons, low-carbon alloy steels were developed that produce a tempered martensitic structure when quenched and bainitic structures when cooled at slower rates. A low-carbon steel can offer four potential benefits (Ref 2, 3):

- High toughness (low impact transition temperature)
- Improved weldability and more efficient solution and precipitation of carbonitrides
- High dislocation density, which can lead to higher strengths
- Elimination of post-heat treatment

Initially, low-carbon bainitic steels were not very popular because of strength limitations. At the time, austenitic grain refinement and accelerated cooling were fairly undeveloped procedures; currently, however, both are accepted practices in the steel industry. This work was undertaken to study the reheat response of a low-alloy steel and the use of an atomizer as a novel tool for achieving a variety of accelerated rates, thus allowing control of structure and properties.

2. Accelerated Cooling of Steels

2.1 *Advantages of Atomizers for Accelerated Cooling*

Rapid cooling by quenching poses significant heat-transfer problems. The temperature of the workpiece is often much higher than the saturation temperature of the liquid, and thus heat transfer is often by film boiling. Also, the temperature of the surface is higher than the coolant by as much as 50 to 1000 K. In such cases the quenching process results in a vapor blanket surrounding the specimen, which also leads to film boiling (Ref 4, 5). Therefore, relatively slow cooling occurs at elevated temperature as heat transfer takes place by radiation through

S.R. Pejavar and **P.B. Aswath,** Mechanical and Aerospace Engineering Department and Materials Science and Engineering Program, University of Texas at Arlington, Arlington, TX 76019

the vapor film. In addition, the surfaces of the workpiece are blunt and knowledge of the heat-transfer rate on a curved surface is needed.

An alternative to quenching is the use of a water spray system. In this process, a spray of water is used to cool the forgings on a conveyor belt, which can significantly increase productivity (Ref 6). Water spraying has some disadvantages, chief among them being that the efficiency of cooling is low because the heat-transfer rates do not always increase with an increase in the volume of water being sprayed. The water droplets are large, leading to localized film boiling and a reduced water evaporation rate. In addition, water sprays cover relatively small areas, leading to localized rapid cooling and the formation of quench cracks. Lastly, water sprays are invariably nonuniform.

A more attractive alternative involves the use of an atomizer, which combines air and water to form a fine mist. In an atomizer, a jet of water combines with a jet of air to produce an air/water mixture that is directed toward the workpiece in a plume of mist. The air plays a dual role, atomizing the water into fine droplets and carrying the fine droplets to the workpiece with a high velocity. The primary advantages of the use of an atomizer include:

- The jet has a high kinetic energy, and thus a larger fraction of atomized water comes in contact with the specimen. In addition, a larger area of heat exchange is covered due to the dispersion of the water droplets in the form of a solid cone.
- The water droplets are of a very fine size, and any water that is not vaporized upon contact with the hot metal descends as a fine mist, forming an ambient cooling zone.
- Cooling is homogeneous and uniform because of the uniform distribution of water droplets around the workpiece.
- The velocity, distribution, and volume fraction of air and water in the jet from the atomizer can be controlled with great flexibility by varying the flow rate of water, air, or both. The atomizer system can be used with minor modification for a variety of workpieces and compositions.
- Controllability of the surface heat flux is the greatest single advantage.

Spray cooling using a single-phase fluid is not new and has been suggested for a variety of applications. Recently, spray boiling has been proposed for microelectronic devices with high-power dissipation rate (Ref 7-10). A comprehensive literature survey for jet impingement cooling is provided by Konechni (Ref 11). In a majority of reported work, the spray is being introduced to a flat surface whose temperature is not extremely higher than the coolant (e.g., see Ref 8 and 12). Information regarding binary spray mixtures, especially for cooling high-temperature surfaces, is lacking. This technique offers a tremendous opportunity to develop a fundamental framework to study both the heat-transfer and metallurgical aspects of cooling of rolled and forged components.

2.2 *Basic Issues in Heat Transfer*

An ideal case of heat transfer involves the use of a medium that can instantly remove the heat from the surface of the part. In such situations the rate of cooling is controlled by the rate at which the heat is able to diffuse from the interior of the part to the surface. However, most practical mediums are unable to provide this infinite quench. In practice, cooling rate is a function of several variables, including velocity, density, and viscosity of the fluid, as well as the different mechanisms of boiling, which include a nucleate boiling regime, a transition boiling regime, and film boiling.

In generalized form, the heat transfer from parts can be written in the form of Newton's Law of Cooling, given by:

$$q = hA\,(T_1 - T_2) \qquad \text{(Eq 1)}$$

where q is the rate of heat transfer, A is the surface area in contact with liquid, T_1 is the surface temperature of the part, T_2 is the fluid temperature away from the surface, and h is the heat-transfer coefficient.

The actual heat flow from the interior of a part to its surface can be determined by Fourier's equation:

$$q = k_s A \frac{dT}{dx} \qquad \text{(Eq 2)}$$

where q is the amount of heat transferred, k_s is the thermal conductivity of the part, A is the surface area of the part, and dT/dx is the thermal gradient. In addition, the thermal conductivity, k_s, of the steel can be related to the heat-transfer coefficient, h ($h = h_R + h_C$), yielding a dimensionless heat-transfer coefficient or Biot's number (B), which is given by:

$$B = \frac{hD}{k_s} \qquad \text{(Eq 3)}$$

where h_R is the heat-transfer coefficient due to radiation and h_C is the heat-transfer coefficient due to convection.

It should be noted that during the quenching of steel parts, the flow of quenchant at the surface is turbulent. Flow past irregularly shaped parts is not well defined, and analytical expressions are difficult to determine. Experimental approaches typically are used. The rates of heat removal from a part cooled by quenching in water and from one cooled by an atomized spray of air/water would show some significant differences. The boiling curve for saturated water at atmospheric pressure on a flat horizontal heater is shown in Fig. 1(a) (Ref 13). Each individual region of this curve is discussed in terms of mechanisms of boiling when quenched and compared to probable mechanisms of heat transfer in the atomized air/water spray. Figure 1(b) shows typical cooling rates and heat flux as a function of wall flux when an atomized mist of air/water is used to cool a solid cylindrical block.

2.3 *Comparison of Heat-Transfer Mechanism in Pool Boiling and Atomized Spray*

The rate of heat transfer as a function of superheat ($T - T_{sat}$) is shown in Fig. 1(a) for pool boiling (Ref 13). T_{sat} is the saturated boiling temperature of water (~373 K at 1 atm). The four primary regions of heat transfer are natural convection, nucle-

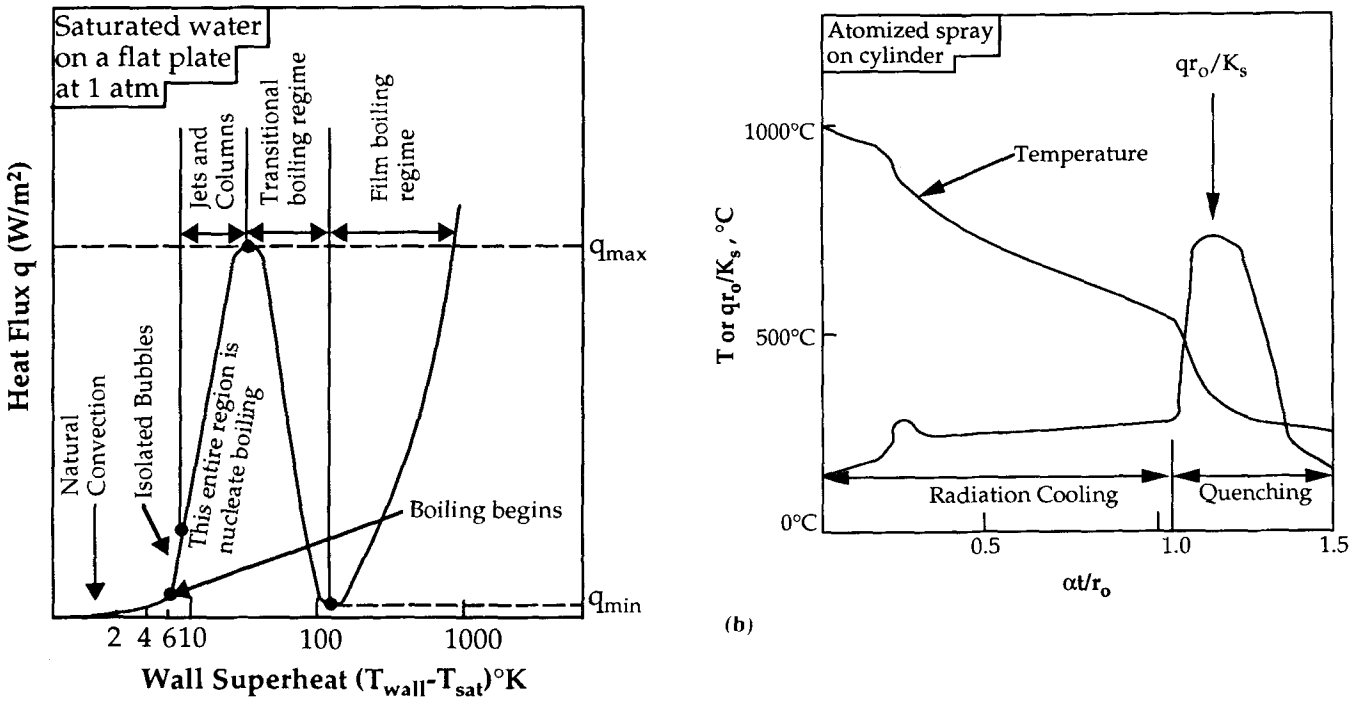

Fig. 1 (a) Typical pool boiling curve, indicating the different regimes of boiling. (b) Typical cooling curve when a solid cylinder is cooled with an atomized spray of air/water, with temperature or normalized heat flux plotted as a function of nondimensional time. q, heat flux; r_0, radius of the cylinder; K_s, thermal conductivity; α, diffusivity; and t, time

ate boiling, transitional boiling, peak pool boiling, and film boiling.

2.3.1 Natural Convection

Water that is not in contact with its own vapor does not boil at the normal boiling points, T_{sat}. However, the temperature of water continues to rise until bubbles form. On conventional machined surfaces this happens when the surface is just a few degrees above T_{sat}. When a part is cooled from high superheats with the aid of an air/water spray with ultrafine droplets, it can be postulated that radiation effects from the part provide sufficient heat to form a vapor phase surrounding the part. Hence, heat transfer by natural convection would be reduced or nonexistent at very high temperatures. At lower temperatures, natural convection will dominate heat transfer.

2.3.2 Nucleate Boiling

This is a characteristic mechanism involved in heat transfer during the nucleation of bubbles of vapor at the metal/liquid interface during the normal quenching process. This occurs at low superheat of 2 to 30 K and is a manifestation of the quenching process. There are two characteristic regimes in nucleate boiling. First is an early bubble nucleation regime at low superheats of 4 to 10 K, where the heat flux is approximately given by:

$$q_N \propto \Delta T^a n^b \qquad \text{(Eq 4)}$$

where $\Delta T = T_w - T_{sat}$, $a \sim 1.2$, and $b \sim 0.33$. In the second regime, bubble coalescence and slug formation occur at 10 to 30 K superheat. When a part is cooled with the aid of an atomized air/water spray, water droplets are instantly vaporized on contact with the metal, with no need for nucleate boiling. Nucleate boiling can play a role in atomized spray cooling only at low superheats and/or large flow rates if a film of water forms on the surface of the part.

2.3.3 Transitional Boiling

In the pool boiling mechanism, the heat flux diminishes as the superheat is further increased and the efficiency of the vapor escape process worsens. This occurs when the hot surface becomes completely blanketed in vapor and heat flux reaches a minimum, q_{min}. This region is of little practical interest due to its inherent instabilities and low heat flux. When an air/water atomized mixture is used, the high-velocity droplets can penetrate the vapor blanket and reach the surface of the part, and hence this region is minimized. It has been shown by Haji-Shiekh et al. (Ref 14) that the radiation coming to a droplet, q_r, can be expressed by:

$$q_r = \pi r_d^2 F_{d-c} \varepsilon \sigma T^4 \qquad \text{(Eq 5)}$$

where ε is the emissivity of the cylinder, r_d is the radius of the droplet, F_{d-c} is a shape factor between the projected area of droplet and cylinder, and T is the temperature of the workpiece. A portion of this energy is absorbed by the droplet, causing it to

Table 1 Chemical composition of the HSLA steel

Composition, wt%										
C	Mn	P	S	Si	Cu	Ni	Cr	Mo	V	Nb
0.1-0.18	1.65-2.0	0.03 max	0.03 max	0.5-0.7	0.35 max	0.2 max	0.2 max	0.15-0.2	0.02 max	0.09-0.12

evaporate. Neglecting the evaporation by convection, the following is valid:

$$\rho_\omega \frac{dV_d}{dt} h_{fg} \cong \alpha_\omega q_r \qquad \text{(Eq 6)}$$

where h_{fg} is the enthalpy of evaporation, V_d is the volume of the droplet, α_ω is the absorptivity of water, and ρ_ω is the density of water. Assuming a spherical droplet of radius r_d, this equation can be further reduced to:

$$\frac{dr_d}{dt} \cong \frac{\alpha_\omega \varepsilon \sigma T^4}{4\rho_\omega h_{fg}} \qquad \text{(Eq 7)}$$

This indicates that the rate of change of the radius of the droplet is independent of droplet size. Hence, small droplets can potentially evaporate before reaching the surface. By judicious control of the droplet size, it is possible to control the cooling rate. For example, if slow cooling at high temperature followed by rapid quenching is desired, it is possible to use small droplets initially and then larger droplets.

2.3.4 Peak Pool Boiling

In pool boiling it is desirable to extract heat by maintaining the superheat at the upper end of the nucleate boiling region, where heat flux is maximum. This region is very unstable, as any small increase in wall superheat leads to a quick decrease in heat flux—a situation that arises in pool boiling due to the large amount of vapor that is formed. The vapor tries to move upward, but does not have a clear escape route. When a large slug of vapor manages to escape to the surface, the liquid water falls in—leading to the formation of another slug. This scenario is avoided when cooling parts with an atomizer, because a continuous liquid phase is eliminated. The vapor that forms due to the evaporation of ultrafine droplets of water is able to leave the surface easily.

2.3.5 Film Boiling

Once a stable vapor blanket is established in pool boiling, the heat flux, q, will increase only with an increase in ΔT. The mechanics of heat removal during film boiling are similar to film condensation. A significant difference between the two is that the heat-transfer coefficient in boiling is much smaller, because the heat must be transferred through a vapor film instead of a liquid film. When an atomized spray of air/water is used, the vapor blanket is broken by the penetration of high-velocity droplets. Hence, the heat-transfer rate is much higher than in pool boiling. The only limitation would occur if the water droplets were to completely vaporize before impinging on the surface of the part; in such a situation, the heat-transfer coefficient would be smaller.

Figure 1(b) shows the heat flux represented as qr_0 / k_s, which has units of temperature as a function of dimensionless time: $\alpha t / r_0^2$ where r_0 is the radius of the cylinder and α is the diffusivity of the metal in square meters per second. At high superheats during the early stages of cooling, the heat flux is primarily due to radiation effects. The droplets are completely vaporized before or at the point of contact with the cylinder. At lower temperatures or higher flow rates, quenching of the cylinder occurs by the formation of a thin layer of water. At this stage a significant amount of phase change can take place at the surface of the cylinder, leading to a much higher level of heat flux. The time at which quenching occurs decreases when larger amounts of water are used.

3. Experimental Procedure

The alloy studied was a low-carbon HSLA steel supplied by Chaparral Steel Company. The chemistry of the steel is given in Table 1; as can be seen, the steel was microalloyed with niobium and vanadium. Figure 2 shows an optical micrograph of the as-received microstructure. The steel was cut from hot-rolled bar stock 32 mm (1.25 in.) in diameter. This project was multifaceted; some of the important issues addressed include the reheat response of the steel, characteristics of the atomizer nozzle, accelerated cooling, and physical and mechanical properties of the cooled bars.

3.1 *Reheat Response*

Grain size as a function of reheating temperature was studied. Samples 1 by 1 by 1 cm in size were subjected to five reheating temperatures of 1173, 1273, 1373, 1473, and 1573 K for ½ h in an argon atmosphere and then quenched in water. The samples were polished and etched in picral. The linear intercept method was used to measure the prior-austenite grain size. On average, 150 readings were taken of each sample, after which the average austenitic grain size was computed. The grain size was measured in each of these cases.

3.2 *Characteristics of the Nozzle*

The pressure jet atomizer used in this study was obtained from Bete Fog Nozzle Inc., Greenfield, MA (BETE 1/4XA-PR150-B). Pressurized air and liquid are mixed internally in an annular region within the nozzle and are expelled together through a single centered round orifice; the energy of compressed air is used to atomize the liquid and to shape the spray pattern. At a constant liquid pressure, the liquid flow rate will be reduced as the air pressure is increased. Increased air consumption results in finer atomization of the liquid.

The selected atomizer was completely characterized for water flow rates of 0.233 kg/min; representative plots are

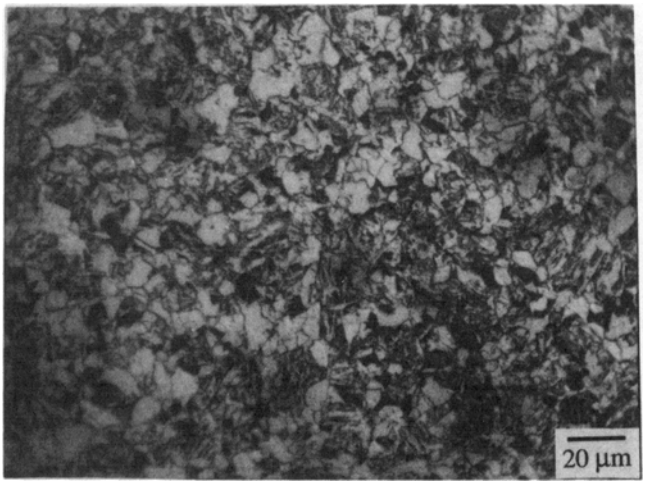

Fig. 2 Optical micrograph of the as-received microstructure of the low-alloy steel bars

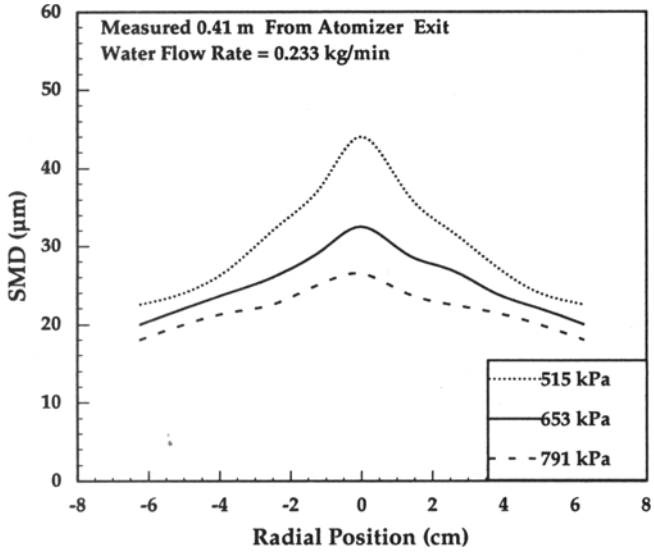

Fig. 3 Radial distribution of droplet size at a distance of 0.41 m from the nozzle for a water flow rate of 0.233 kg/min and various air pressures. SMD, Sauter mean diameter

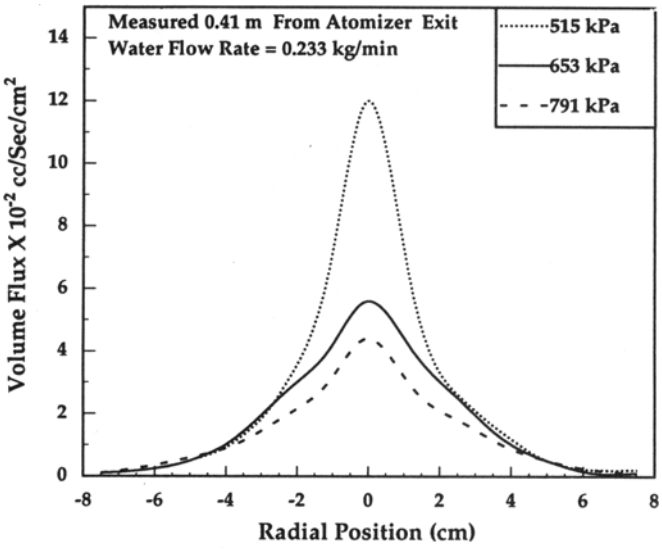

Fig. 4 Radial distribution of volume flux at a distance of 0.41 m from the nozzle for a water flow rate of 0.233 kg/min and various air pressures

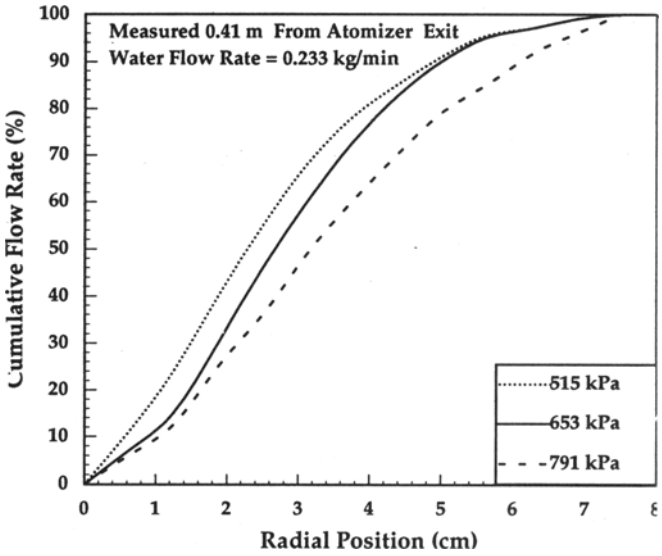

Fig. 5 Cumulative flow rate as a function of radial position at a distance of 0.41 m from the nozzle for a water flow rate of 0.233 kg/min and various air pressures

shown in Fig. 3 to 6. The atomizer produced a single jet of air/water spray that was fully developed at a distance of 0.41 m from the nozzle. The spray was a symmetrical solid cone in shape. The radial distribution of droplet size for a water flow rate of 0.233 kg/min at a distance of 0.41 m from the atomizer exit was characterized for absolute air pressures of 515, 653, and 791 kPa (Fig. 3). At an air pressure of 653 kPa, the distribution of droplets (diameters between 20 and 32 μm) was fairly even. The radial distribution of the volume flux under the same parameters is shown in Fig. 4. At an absolute air pressure of 653 kPa and at a radial position of up to 2.5 cm from the center, the volume flux varied from 2 to 5×10^{-2} cm^3/cm^2. Figure 5 shows the cumulative flow as a function of radius. At an air pressure of 653 kPa, 46% of the flow (0.107 kg/min) was within the first 2.5 cm radius (5 cm diameter). Figure 6 shows the cumulative flow as a function of droplet size. At the same air pressure, 50% of the flow was made up of droplets of a diameter less than 33 μm. It is clear from Fig. 3 to 6 that the atomized spray was fully developed at a distance of 0.41 m from the nozzle exit and that the size and distribution of the water droplets were fairly uniform over a radial distance of about 5 cm.

3.3 *Accelerated Cooling*

Cylindrical samples 10 cm in height and 3.125 cm in diameter were cut, and three holes 2.5 cm deep were drilled. One hole was drilled at the center of the solid cylinder; the other two holes were located 1 mm below the surface, one directly facing

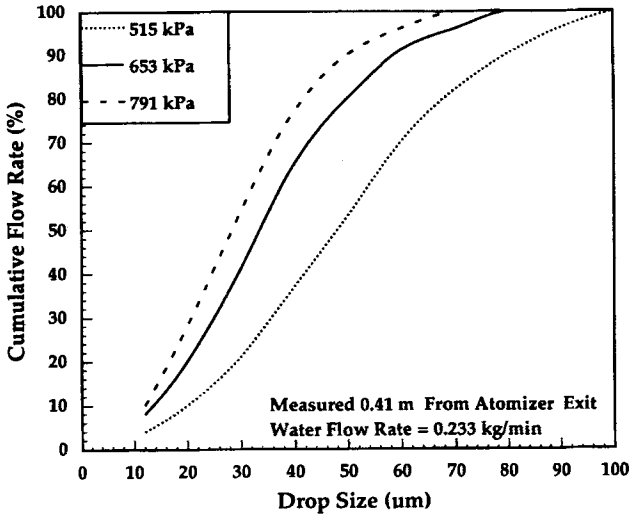

Fig. 6 Cumulative flow rate as a function of water droplet size at a distance of 0.41 m from the nozzle for a water flow rate of 0.233 kg/min and various air pressures

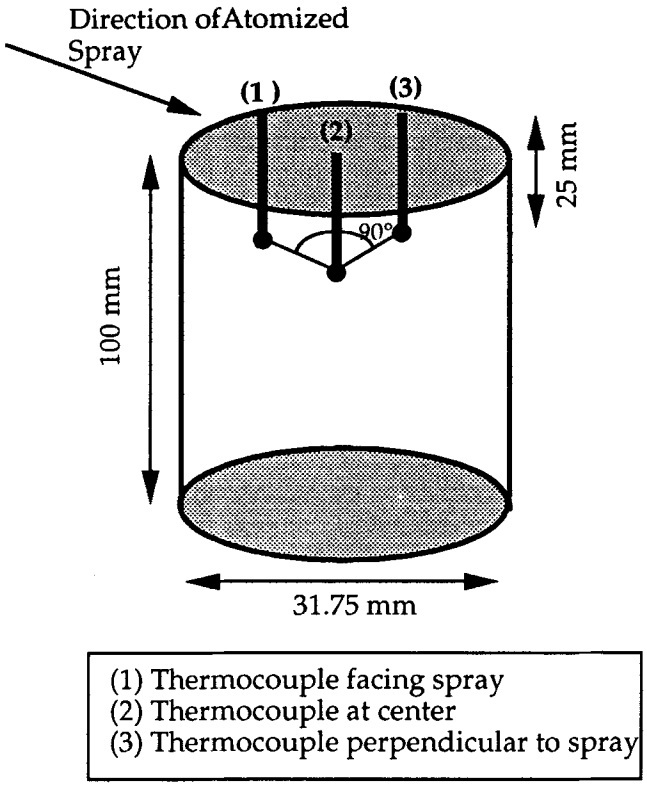

Fig. 7 Schematic of the sample geometry showing the location of the thermocouples

the spray and the other perpendicular to it. Thermocouples were embedded in these holes at a depth of 25 mm and glued using high-temperature cement. Figure 7 schematically depicts the geometry of the sample.

The sample was then heated to 1283 K before being subjected to any one of various cooling programs using the atomizer. A schematic of the experimental setup used to cool the cylindrical sample is shown in Fig. 8. An air compressor and a water pump were used to achieve a constant absolute air pressure of 666.7 kPa and a water pressure of 689 kPa. A Dwyer Instruments flow meter was used to monitor the water flow rate. A Sierra Top Trak (Sierra Instruments, Inc., Monterey, CA) flowmeter was used to measure the pressure drop of air.

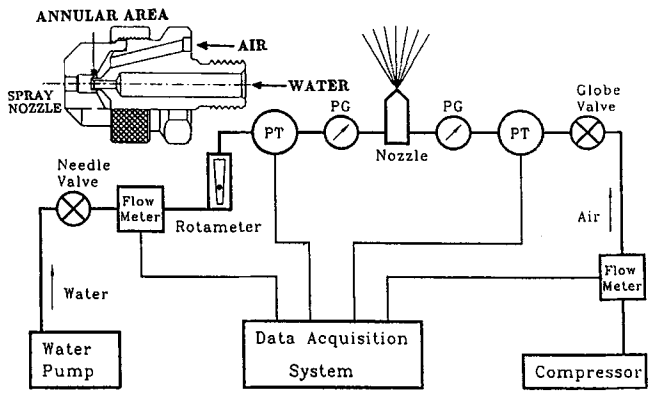

Fig. 8 Schematic of experimental setup used in the accelerated cooling of the steel bars. PT, pressure transducer; PG, pressure gage

Table 2 Atomizer water flow rates and corresponding average cooling rates of the steel bar in the temperature range of 1073 to 673 K

Water flow rate, kg/min	Air pressure	Average cooling rate, *K*/min
0.504	666.7	470
0.378	666.7	450
0.251	666.7	415
0.189	666.7	275
0.126	666.7	145
0.063	666.7	110
Quenched	...	1440

The temperatures from the thermocouples were recorded throughout the test using a Hewlett Packard data acquisition system model 3852A (which has 80 channels of input and a 4-channel analyzer) at intervals of 0.1 s, and the cooling profile for each program was obtained. The various cooling programs used were listed in Table 2, along with the approximate cooling rates. The average cooling rates were calculated between 1073 and 673 K.

3.4 *Microstructure, Mechanical Tests, and Fractography*

The polished samples were prepared for optical microscopy by etching with nital to reveal the microstructure. The test samples were machined from the midradius and center of the cylindrical sample after they had been subjected to the different cooling programs. Tensile, Charpy, and Rockwell C hardness tests were conducted. Tensile samples were machined and tested as per ASTM standards E23 (Ref 15) and Charpy samples as per ASTM standard E8 (Ref 15). The fractured surfaces

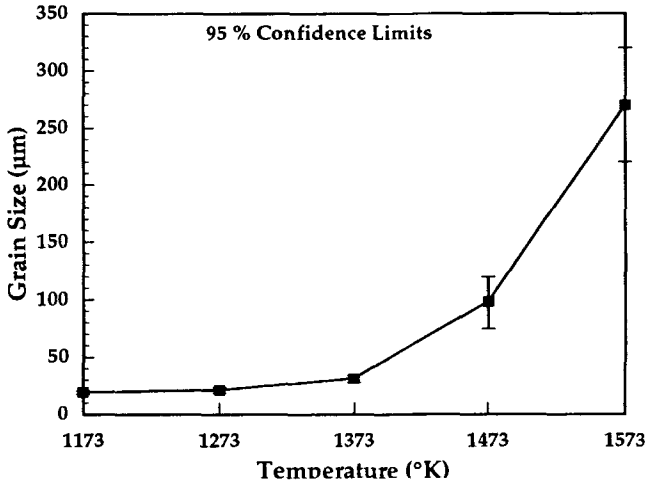

Fig. 9 Prior-austenite grain size as a function of reheating temperature after being held at each temperature for 0.5 h in an argon atmosphere and then quenched

obtained from the tensile and Charpy V-notch tests were examined using scanning electron microscopy (SEM). The fractographs were then analyzed to determine the mechanism of fracture.

4. Results and Discussion

4.1 *Reheating Response*

The response of austenite to reheating has been a subject of extensive study (Ref 16-19). Austenite conditioning, as it is commonly called, is a standard feature in the forging and steel industries. This is because the steel must be reheated to austenitizing temperatures before being subjected to the hot-working operation.

Too low a reheating temperature (~1173 K) is not favored by industry because of the greater power needed to work the steel due to its lower plasticity (Ref 20). This also causes greater wear and tear on forging dies and on rolling mill equipment. A fine austenite grain size yields a larger ratio of boundary to volume and thus a larger number of nucleation sites for ferrite during the γ/α transformation. This leads to a finer ferrite grain size. Too high a reheating temperature (e.g., ≥1523 K) also is not favored. In this case, all the carbonitrides either dissolve in austenite or coarsen at a rapid rate (Ref 20, 21), leading to rapid austenite grain coarsening.

The stability of austenite grain boundaries at high temperatures is ensured if precipitation occurs at as high a temperature as possible and the precipitate is sufficiently fine to pin the austenite grain boundaries (Ref 22). Niobium and titanium are the two most common microalloying elements added to refine austenite grain size. Vanadium, niobium, and titanium all have limited solubility in austenite; as the temperature drops, they precipitate out as carbides or carbonitrides. It has been ascertained by many investigators (Ref 1, 23-25) that vanadium precipitation takes place at about 1173 K because of its greater solubility in austenite and thus does not participate in austenite grain refinement. Vanadium contributes toward precipitation hardening at lower temperatures. On the other hand, the solubility of niobium is lower than that of vanadium; therefore, niobium precipitates out at higher temperatures (~1523 K) in austenite. These niobium precipitate particles pin the austenite grain boundaries and prevent austenitic growth.

The austenitic grain size of Microtuff-15™ (Specialty Minerals, Inc., New York, NY) steel as a function of reheating temperature for a constant time of 0.5 h is shown in Fig. 9. The grain size of austenite increases by less than 15 μm as the temperature is increased from 1173 to 1373 K. Beyond 1373 K grain growth is rapid, with maximum growth at 1573 K. At all temperatures below 1173 K, both niobium and vanadium are effective in preventing grain growth. At temperatures greater than 1273 K, appreciable grain growth occurs, and at 1373 K the austenite grain size is 25 μm. The solubility of niobium in austenite is a strong function of carbon content (Ref 26, 27). For example, at 1523 K, a 0.4% C steel can retain 0.02% Nb in solution, whereas in a 0.1% C steel 0.07% Nb is soluble. The presence of manganese also increases the solubility of niobium in austenite at $T > 1373$ K. At $T > 1373$ K preferential dissolution of the finer precipitates can occur, leaving behind coarser precipitates and thus reducing the efficiency of grain-boundary pinning. At $T = 1473$ K the grain size is approximately 120 μm. The microstructure exhibits a duplex microstructure with a few large grains and some small grains and corresponds to an abnormal grain-growth regime (Ref 28). At $T = 1573$ K the grain size is approximately 270 μm. It is safe to speculate that all the niobium is in solution and normal grain growth has resumed. All of our experiments in accelerated cooling involved heating to 1283 K to approximate the finish temperature in hot forging. At this temperature there is little or no grain growth for short hold times.

4.2 *Thermal History of the Samples*

The cooling profiles of the bar quenched in agitated water and the bars cooled using an atomizer with water flow rates of 0.504, 0.189, and 0.063 kg/min are shown in Fig. 10(a), 11(a), 12(a), and 13(a), respectively. A constant absolute air pressure of 666.7 kPa was used in samples cooled with an atomizer. The corresponding microstructures obtained are shown in Fig. 10(b), 11(b), 12(b), and 13(b), respectively. The cooling curves represent the variation of temperature as a function of time (solid lines) and the variation of cooling rate as a function of temperature (dashed lines). The average cooling rate for the quenching process was 1430 K/min. The cooling rates were computed between 1073 and 673 K using the formula $\Delta T/\Delta t$, where ΔT is the temperature interval and Δt is the time interval (these calculations were done at 1 s intervals). It is immediately apparent from the quenched sample that cooling rates as high as 4500 K/min were achieved near the surface of the specimen. At approximately 785 K the cooling rate dropped to a minimum, followed by a rapid increase. This region may correspond to a vapor blanket/film boiling region. This phenomenon is transitory in nature, as agitation aids in the removal of bubbles from the specimen surface. The center of the sample exhibited fairly uniform cooling.

When cooled at a water flow rate of 0.504 kg/min, the cooling rate of the thermocouple facing the spray was much higher than that of the interior thermocouple. The irregular nature of

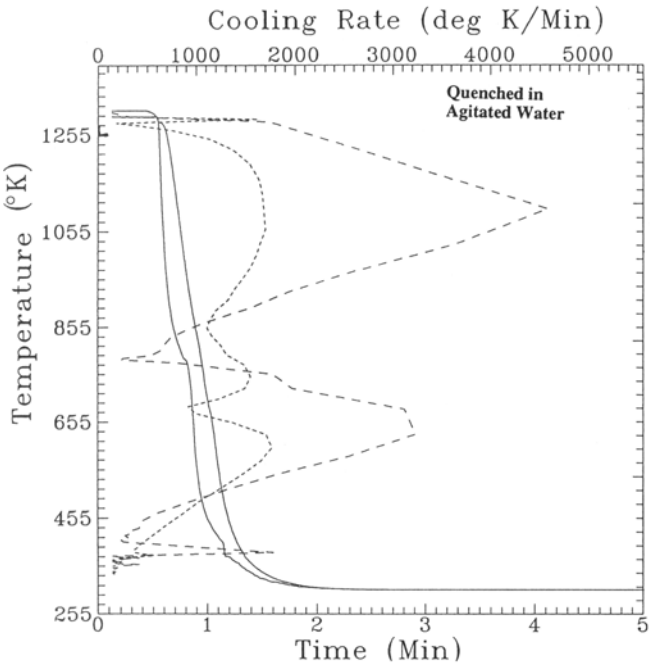

(a)

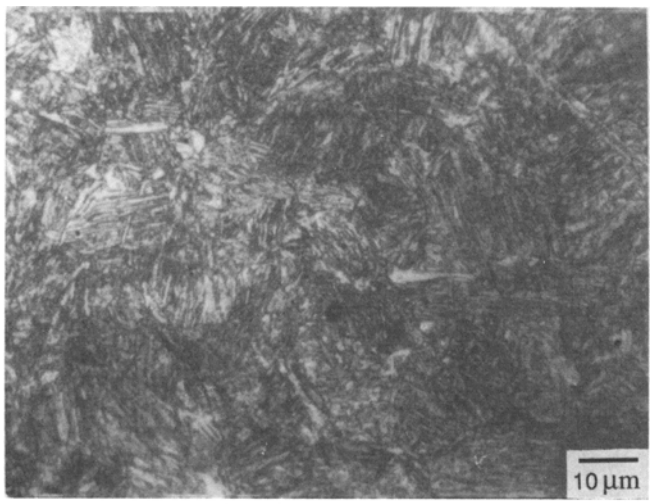

(b)

Fig. 10 (a) Temperature versus time (solid lines) and cooling rate versus temperature (dashed lines) profiles for a sample quenched in water. The longer dashes correspond to the thermocouple at the surface, and the shorter dashes correspond to the thermocouple in the center. (b) Microstructure obtained for the cooling program at the center of the sample

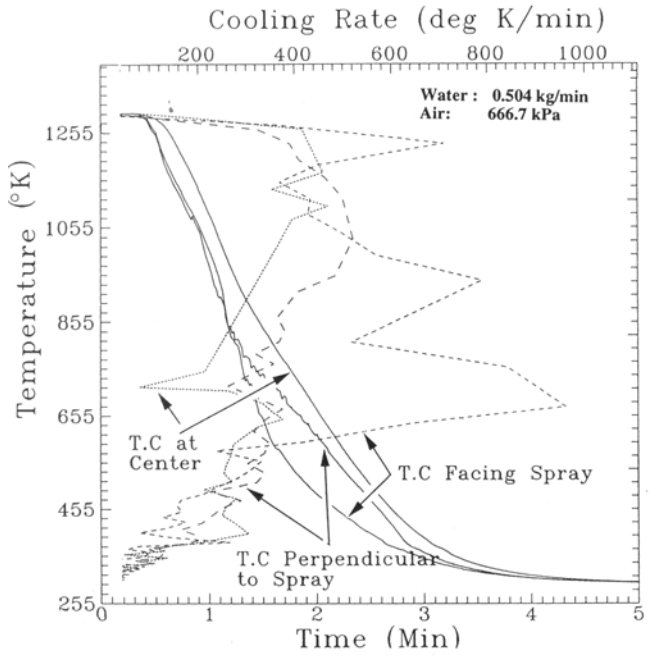

(a)

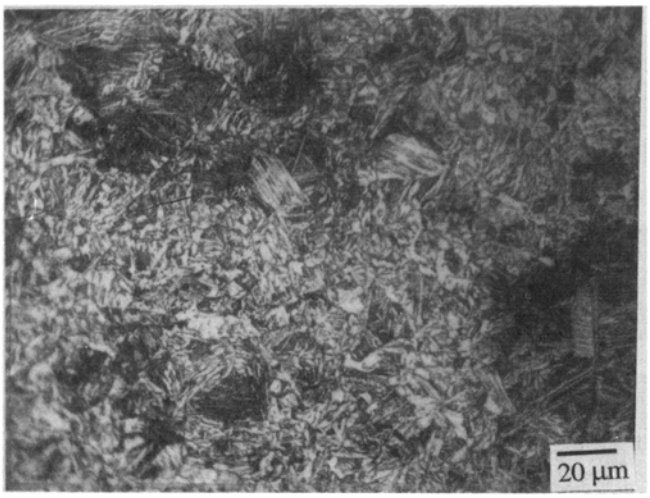

(b)

Fig. 11 (a) Temperature versus time (solid lines) and cooling rate versus temperature (dashed lines) profiles for a water flow rate of 0.504 kg/min and an absolute air pressure of 666.7 kPa. The longest dashes correspond to the thermocouple perpendicular to the spray, the shortest dashes correspond to the thermocouple in the center, and the intermediate-size dashes correspond to the thermocouple facing the spray. (b) Microstructure obtained for the cooling program at the center of the sample

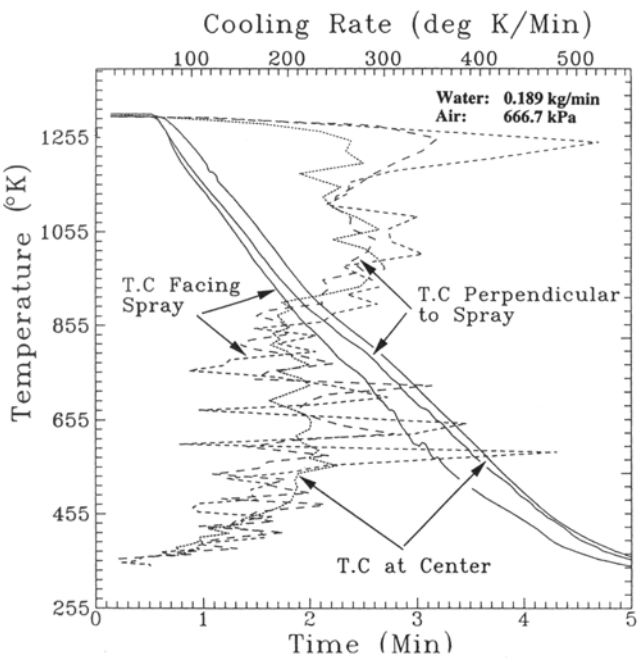

(a)

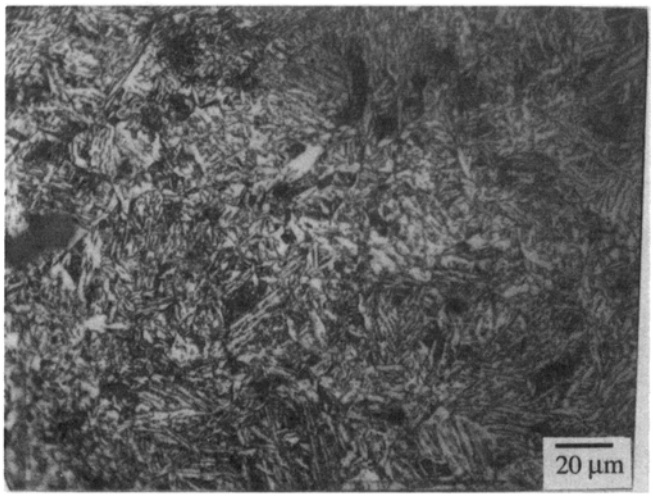

(b)

Fig. 12 (a) Temperature versus time (solid lines) and cooling rate versus temperature (dashed lines) profiles for a water flow rate of 0.189 kg/min and an absolute air pressure of 666.7 kPa. The longest dashes correspond to the thermocouple perpendicular to the spray, the shortest dashes correspond to the thermocouple in the center, and the intermediate-size dashes correspond to the thermocouple facing the spray. (b) Microstructure obtained for the cooling program at the center of the sample

the temperature versus time curve is reflected as spikes in the cooling rate versus temperature curve. The same scenario is reflected in the curves corresponding to the thermocouple that was situated perpendicular to the spray. It can also be postulated that the sharp spikes in the cooling rate curves, especially for thermocouples facing the spray and perpendicular to the spray, may be due to sudden increases in heat-transfer rate. Initially, as the temperature of the surface is high, higher cooling rates are obtained. Due to the formation and delamination of the oxide scale on the surface, the cooling rate drops. However, the high velocity of the spray can knock away any oxide scale that forms, leading again to improved cooling. On the other hand, the cooling curve for the thermocouple at the center of the sample was smooth and showed no sudden changes in cooling rate. In the temperature range from 1073 to 673 K, the cooling rate was approximately 470 K/min in the center of the sample.

At a water flow rate of 0.189 kg/min, the cooling rate for the thermocouple facing the spray was much smaller than the comparable cooling rate when 0.504 kg/min water flow was used. Again, the spikes in the cooling curves may be attributable to sudden increases in heat-transfer rate. A water flow rate of 0.189 kg/min produces a smaller volume of water as well as a finer drop size, and cooling rate is a function of both of these factors. The radiation from the hot cylinder could have easily vaporized the droplets, delaying the quenching phenomenon and slowing the cooling rate. The thermocouples facing the spray, perpendicular to the spray, and at the center of the sample exhibited almost the same cooling rates of 275 K/min in the temperature range from 1073 to 673 K. Because the cooling processes were slower, thermal conduction had time to occur, which helped to even out the temperature. It is important to note that, except for a few initial spikes in the cooling rate, the overall rates were fairly steady over time.

At a water flow rate of 0.063 kg/min, all three thermocouples exhibited the same cooling rates (~110 K/min), with the thermocouple facing the spray showing an initial increase to nearly 600 K/min before dropping. There was also a change in slope of the cooling curves of the thermocouples perpendicular to the spray and at the center of the sample. This occurred at approximately 860 K. At temperatures greater than 860 K, the primary mode of heat transfer was radiation with a bit of convection. This is because the fine droplets were vaporized before they reached the surface. At temperatures lower than 860 K, wetting of the surface takes place, leading to the evaporation/boiling mechanism of heat transfer. The wetting temperature is higher for higher flow rates because of the larger volume of water and larger drop size. The drops are not vaporized by the time they reach the surface and so are able to wet the surface at higher temperatures. The average cooling rates at both the center and the surface were approximately 100 K/min in the temperature range of 1073 to 637 K, indicating a fourfold decrease in cooling rate compared to the sample cooled with 0.504 kg/min water and a 13-fold decrease in cooling rate compared to the sample quenched in agitated water.

4.3 *Microstructure*

The as-received microstructure of the low-carbon steel is shown in Fig. 2. The microstructure consists mainly of ferrite and pearlite, with ferrite being the predominant phase. This mi-

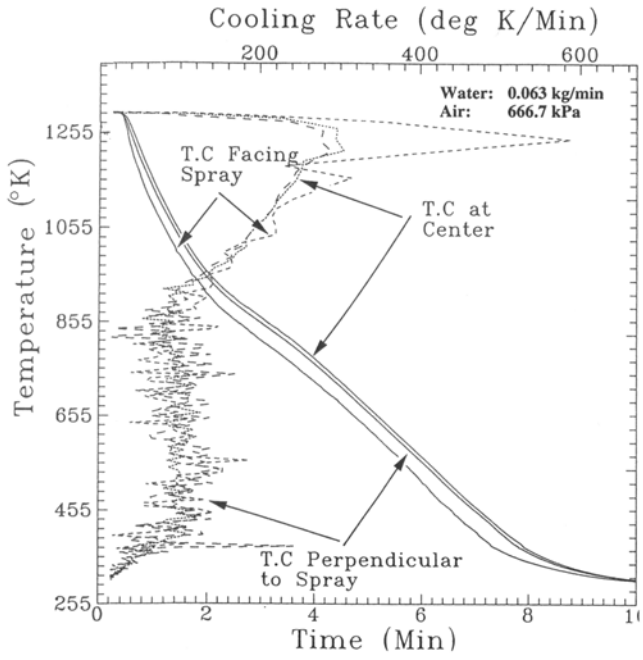

(a)

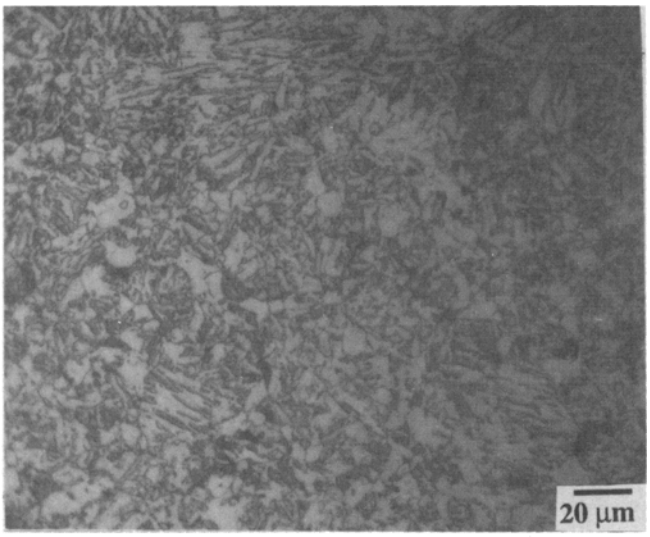

(b)

Fig. 13 (a) Temperature versus time (solid lines) and cooling rate versus temperature (dashed lines) profiles for a water flow rate of 0.063 kg/min and an absolute air pressure of 666.7 kPa. The longest dashes correspond to the thermocouple perpendicular to the spray, the shortest dashes correspond to the thermocouple in the center, and the intermediate-size dashes correspond to the thermocouple facing the spray. (b) Microstructure obtained for the cooling program at the center of the sample

crostructure is formed due to air cooling after the hot-rolling operation. The fine austenitic grain size is brought about by niobium additions, which precipitate out as carbonitrides and pin the austenite grain boundaries. In addition, the hot-working operation deforms the prior-austenite grains, creating further inhomogeneities and thereby increasing the number of ferrite/pearlite nucleation sites.

Figure 10(b) shows the microstructure obtained at the center of the cylinder quenched in agitated water. The microstructure exhibits a tempered martensitic structure, which is the characteristic feature of this steel. As the martensitic transformation is completed at a high temperature ($M_f > 478$ K), it is subjected to autotempering.

In the other cooling programs with water flow rates of 0.504 kg/min and below, a bainitic structure results (Fig. 11b), which is the microstructure obtained from the center of the sample cooled with a water flow rate of 0.378 kg/min. The microstructure is primarily bainite, with some islands of martensite. When a flow rate of 0.189 kg/min is used, a completely bainitic microstructure is obtained (Fig. 12b). At smaller flow rates of 0.063 kg/min, a mixture of upper bainite and ferrite is seen (Fig. 13b).

Bainite transformation product in this steel is promoted by the presence of molybdenum and niobium, with molybdenum being the more effective element. Many investigators (Ref 19, 29) have shown that molybdenum and niobium suppress polygonal ferrite formation and promote an acicular product. Molybdenum, niobium, and nickel also ensure that the bainite "C" curve has a flat top so that bainite forms over a wide range of cooling rates. The formation of bainite is also promoted by accelerated cooling (Ref 30). It has been shown (Ref 31) that increasing the cooling rate up to a certain limit does not change the ferrite start temperature range (1048 to 1063 K) and the bainite transformation temperature range (833 to 713 K), but there is less time for ferrite transformation to take place. Hence, an increasing amount of transformation will take place in the bainite transformation range. Further increasing the cooling rate narrows the bainite transformation range, and martensite transformation occurs.

Because of fine prior-austenite grain size and because accelerated cooling lowers the γ/α transformation temperature, all of the microstructures are fine grained (Ref 2, 30, 32, 33). Lowering the transformation temperature increases the amount of supercooling, which leads to a larger number of nucleation sites for the α phase and hence a fine structure. Accelerated cooling is seen to be more effective than nickel or manganese in grain refinement through lowering of the transformation temperature (Ref 32).

4.4 *Mechanical Properties*

Even though the tensile strength values of bainitic steels subjected to accelerated cooling are less than normal quenched and tempered steels, they have much better toughness and overall provide a much better combination of strength and toughness. The strength increments in this steel brought on by accelerated cooling are primarily due to the formation of a fine dispersion of bainite (since pearlite and ferrite formation is suppressed) and to precipitation hardening. The addition of molybdenum also increases yield strength and tensile strength—by 3 and 4.5 ksi, respectively. The principal microstructural effect of molybdenum is to alter the morphology of the pearlite and in-

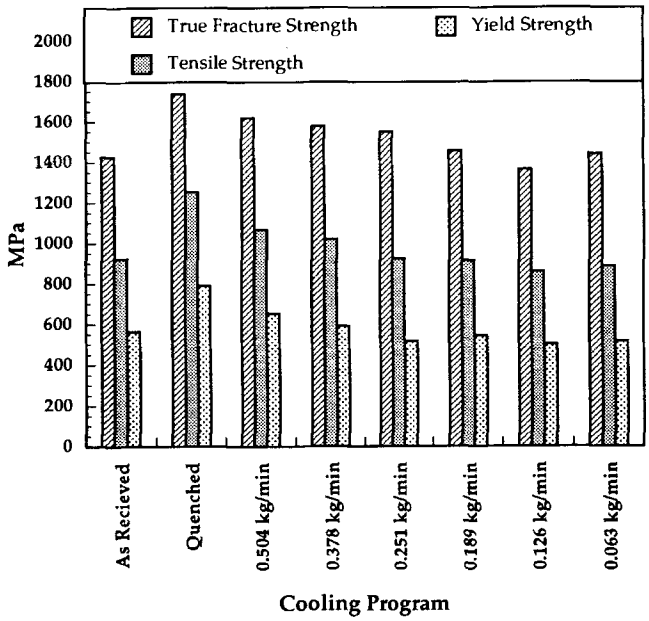

Fig. 14 Variation of 0.2% offset yield strength, ultimate tensile strength, and true fracture strength of the steel bar cooled at various water flow rates but at a constant air pressure of 666.7 kPa. Strength values for the as-received sample and quenched sample are also included.

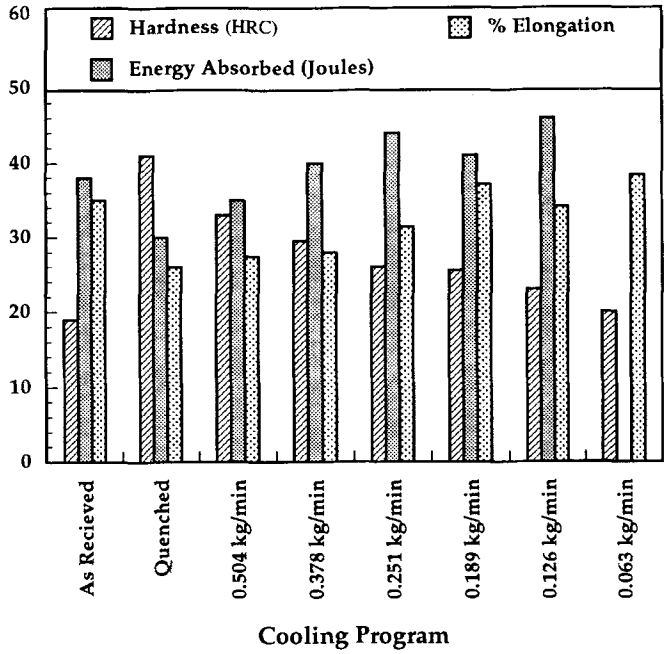

Fig. 15 Variation of percentage elongation, Charpy V-notch impact toughness, and Rockwell C hardness as a function of water flow rate for a constant air pressure of 666.7 kPa

troduce upper bainite as a partial replacement for pearlite. Molybdenum also serves as a solid-solution hardener and enhances the Nb(CN) precipitation.

This steel, like other bainitic steels, exhibits deformation behavior different from that of conventional low-carbon ferrite-pearlite steels (Ref 21, 34)—showing continuous yielding rather than discontinuous yielding. As discussed by Tanaka (Ref 34), when the second phase is pearlite produced by diffusional transformation, the stress-strain curve is discontinuous—resulting in a large yield drop. On the other hand, when the second phase is produced by lattice transformation, the stress-strain curve becomes continuous due to the large number of mobile dislocations generated during the lattice transformation. These steels also exhibit higher strain-hardening rates and greater amounts of uniform deformation during tensile deformation than ferrite-pearlite steels.

4.4.1 Tensile Tests

The data presented here are an average of three tests. The variation of ultimate tensile strength (UTS) with cooling rate is shown in Fig. 14. Quenching (cooling rate, 1440 K/min) produced the highest strength level (1250 MPa). This is directly attributable to the tempered martensitic structure. The strength level decreased as the water flow rate (or cooling rate) decreased, and the microstructure correspondingly moved from bainite plus martensite to completely bainitic at a water flow rate of 0.189 kg/min (cooling rate, 275 K/min). At this cooling rate the UTS was 900 MPa. Further decreasing the water flow rate produced coarser bainitic structures, resulting in a drop in strength. Water flow rates below 0.126 kg/min (cooling rate, 145 K/min) did not affect UTS levels in any significant way.

The variation of true fracture strength with water flow rate is also shown in Fig. 14. This property was highest for the quenched sample (cooling rate, 1440 K/min) and then decreased with decreasing water flow rate. The true fracture strength for the 0.063 kg/min sample (cooling rate, 110 K/min) was higher than for the 0.126 kg/min sample (cooling rate, 145 K/min). The microstructure of the sample cooled with 0.126 kg/min water had some upper bainite, which is known to decrease strength and toughness values.

The variation of 0.2% offset yield strength with cooling rate is also shown in Fig. 14. The trend is similar to the UTS variation. The highest offset yield strength (800 MPa) was exhibited by the quenched sample (cooling rate, 1440 K/min); this property decreased with decreasing cooling rate and reached a minimum value of 525 MPa for the sample cooled with a water flow rate of 0.063 kg/min (cooling rate, 110 K/min). However, the offset yield strength values for the higher cooling rates occurred at a higher fraction of the total tensile load. For example, for the quenched sample the yielding occurred at 65% of the maximum load, whereas for the 0.063 kg/min sample the yielding occurred at 55% of the maximum load. This indicates that the more slowly cooled sample exhibited a larger degree of work hardening in the plastic region. It is important to note here that it was possible to change UTS in the range of 1250 to 900 MPa and yield strength in the range of 800 to 525 MPa strictly by changing the flow rate of water. If the air pressure was also changed, it would be possible to control the final strength and microstructure to a larger degree.

Percentage elongation, Charpy V-notch impact toughness, and Rockwell hardness as a function of water flow rate are shown in Fig. 15. The quenched sample and the sample cooled with a water flow rate of 0.504 kg/min (cooling rate, 470 K/min) had elongation values of 26 and 27.4%, respectively. The high values can be attributed to the presence of retained

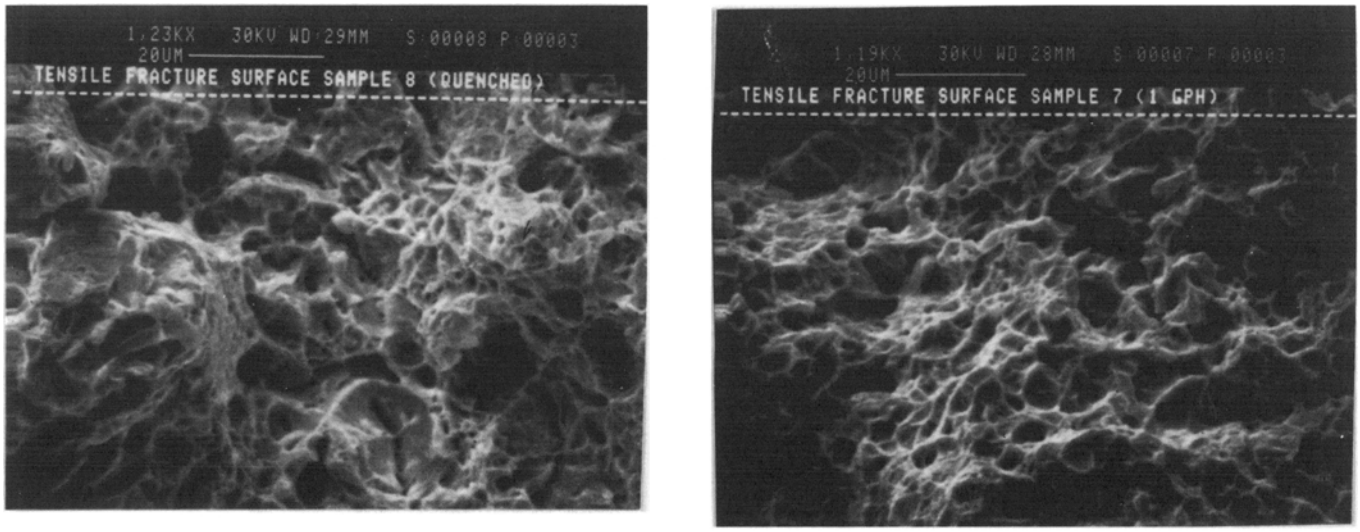

(a) (b)

Fig. 16 SEM micrographs of the tensile fracture surfaces of (a) quenched sample and (b) sample cooled with a water flow rate of 0.063 kg/min and an air pressure of 666.7 kPa

austenite in the microstructure, which contributes to increased plasticity during fracture. The elongation values increased with decreasing cooling rates, reaching a maximum value of 38% for the 0.063 kg/min sample. The elongation value was higher for the 0.189 kg/min sample (cooling rate, 275 K/min) than for the 0.126 kg/min sample (cooling rate, 145 K/min). This discrepancy may be due to some sampling problem.

4.4.2 Tensile Fracture

All the fracture surfaces showed a typical cup and cone type of fracture. This is because even the quenched sample had an elongation value of 26%; the sample cooled with a water flow rate of 0.063 kg/min had elongation of 38%. Fractographs of these two samples are shown in Fig. 16.

The quenched sample (Fig. 16a) exhibited several secondary cracks. These secondary cracks decreased in number with a decrease in cooling rate. The sample cooled with a water flow rate of 0.063 kg/min (Fig. 16b) exhibited no secondary cracks. Both fractographs reveal a dimpled fracture mode. The dimple size for the more slowly cooled sample was much finer compared to the quenched sample, which had larger sized but fewer dimples. The presence of a dimpled fracture surface indicates that fracture proceeded by microvoid coalescence. The localized regions of large ductility in the quenched sample may be attributed to the presence of retained austenite.

4.4.3 Charpy V-Notch Fracture

The variation of Charpy V-notch impact toughness with water flow rate is shown in Fig. 15. As expected, the quenched sample had the lowest toughness value (30 J), with toughness increasing with decreasing cooling rate. The toughness value for the sample cooled with a water flow rate of 0.251 kg/min (cooling rate, 415 K/min) was 45 J and decreased marginally to 41 J for the sample cooled with a water flow rate of 0.189 kg/min (cooling rate, 275 K/min). This is because the 0.251 kg/min sample had a microstructure consisting mainly of lower bainite plus some martensite, whereas the 0.189 kg/min sample had a completely bainitic microstructure that contained small amounts of upper bainite. It is known that upper bainite has poorer impact resistance (Ref 35) than lower bainite, and this may explain the lower toughness value for the 0.189 kg/min sample. Figure 17 shows the Charpy fracture surfaces of the quenched sample and the sample cooled with a water flow rate of 0.063 kg/min. Both samples exhibit a quasi-cleavage type of fracture.

The UTS, yield strength, and Charpy V-notch values for the quenched samples (cooling rate, 1440 K/min) were lower than those reported in the literature (Ref 21) for this particular microalloyed steel. A possible reason for this might be that the values reported in the literature are for samples quenched after the hot-working operation. During hot working, strain-induced precipitation occurs along with the creation of a greater number of heterogeneities in the microstructure, which leads to finer grain-size distribution. The precipitation rate is very sensitive to the level of strain imparted (Ref 1). On the other hand, in this investigation the microalloyed steel was heated to 1283 K before being quenched. The precipitate distribution obtained here would be different, because strain-induced precipitation did not occur. The hot-working finish temperature may be anywhere in the range of 1173 to 1323 K. The hot-working conditions also affect the kinetics of precipitation (Ref 1). For example, rolling to a thinner final gage produces a higher density of smaller precipitates than does rolling to a heavier gage. This might also explain the discrepancy in the strength and toughness levels.

4.4.4 Hardness Tests

The variation of Rockwell hardness number with cooling rate is shown in Fig. 15. The trend here followed the accepted route; that is, it was highest for the quenched sample (41 HRC) and lowest (19 HRC) for the sample cooled with a water flow

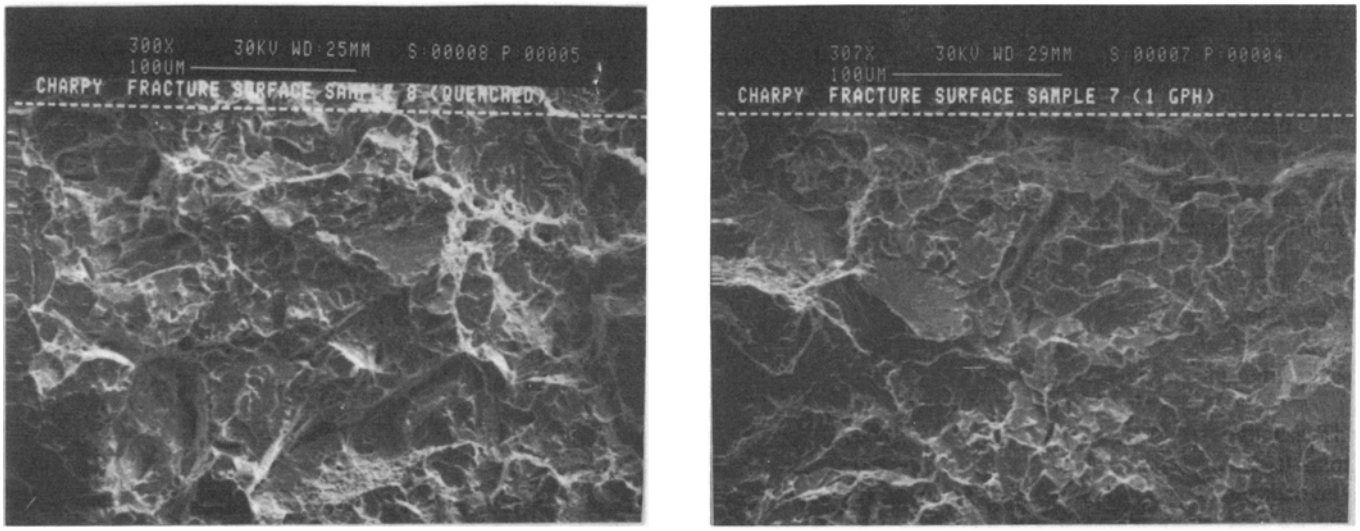

(a) (b)

Fig. 17 SEM micrographs of the Charpy fracture surface for (a) quenched sample and (b) sample cooled with a water flow rate of 0.063 kg/min and air pressure of 666.7 kPa

rate of 0.063 kg/min. The low hardness even for the quenched sample is due both to the low carbon content and to the autotempered martensitic structure. It is important to note here that large variations of mechanical properties can be imparted to a steel by the use of an atomizer with the appropriate air/water mixture.

5. Conclusions

The reheating response of Microtuff-15™ and the effect of accelerated cooling on its microstructure and mechanical properties were investigated. A number of conclusions were reached.

During reheating experiments, grain sizes varying from 19.5 μm at 1173 K to 270 μm at 1573 K were observed. Three regions of grain growth were also identified:

- Normal grain growth from 1173 to 1373 K, where the grain size increased from 19.5 to 31.5 μm
- Abnormal grain growth attributed to secondary recrystallization between 1373 to 1473 K, with grain size increasing from 31.5 μm at 1373 K to 98.6 μm at 1473 K
- Rapid normal grain growth above 1473 K, with the grain size at 1573 K being 270 μm

Tensile strength, yield strength, true fracture strength, hardness, and elongation values of this steel can be varied in a controlled manner by as much as 50% by judicious control of the air/water mixture in the atomizer.

Study of the tensile fracture surfaces of all samples revealed ductile fracture due to microvoid coalescence, with dimple size decreasing with decreasing cooling rate. The quenched sample exhibited the highest number of secondary cracks, while the sample cooled with a water flow rate of 0.063 kg/min exhibited none.

Charpy V-notch impact toughness was lowest for the quenched sample and reached a maximum before decreasing again. The toughness value for the 0.251 kg/min sample was highest (45 J), after which toughness decreased with decreasing flow rate. It can be postulated that the microstructures obtained below water flow rates of 0.251 kg/min contained some upper bainite, which is known to have poorer impact resistance than lower bainite.

One of the primary aims of this study was to develop a unique cooling process using an atomizer. The atomizer proved a very flexible tool for obtaining a variety of cooling rates (from 1440 K/min for the quenched sample to 110 K/min for the sample cooled with a water flow rate of 0.063 kg/min), even though the air pressure was maintained constant at 666.7 kPa. If both the water flow rate and air pressure were varied, much greater flexibility could be obtained.

Acknowledgments

This work was supported in part by Trinity Forge Inc., Mansfield, Texas. Experimental assistance provided by Chaparral Steel and Combustion Associates Inc. is greatly appreciated. Special thanks to Prof. Haji-Shiekh for useful comments throughout this work.

References

1. A.J. DeArdo, J.M. Gray, and L. Meyer, *Niobium 81*, AIME, 1982, p 685
2. F.B. Pickering, *Microalloying 75*, M. Korchynsky et al., Ed., Union Carbide, 1977, p 9
3. T. Gladman, D. Dulieu, and I.D. McIvor, *Microalloying 75*, M. Korchynsky et al., Ed., Union Carbide, 1977, p 32
4. K.-E. Thelning, *J. Heat Treat.*, Vol 3, 1983, p 54-107
5. R.W. Monroe and C.E. Bates, *J. Heat Treat.*, Vol 3, 1983, p 83-99
6. P. Benoit and P. Pithots, BISI-TS 14578, Continuous Casting Conference (Biarritz), IRSID Metals Society, 1976

7. S.C. Yao, S. Deb, and N. Hammouda, in *Heat Transfer in Electronic Equipment,* HTD-Vol 111, American Society of Mechanical Engineers, 1989, p 129-134
8. C.F. Ma and A.E. Bergles, in *Heat Transfer in Electronic Equipment,* HTL-Vol 28, S. Oktay and A. Bar-Cohen, Eds., American Society of Mechanical Engineers, 1983, p 5-12
9. C.F. Ma and A.E. Bergles, *Int. J. Heat Mass Transfer,* Vol 29, 1986, p 1095-1101
10. M. Monde and Y. Furukawa, *Trans. JSME,* Series B, 53-485, 1987, p 199-203
11. S. Konechni, M.S. thesis, University of Texas at Arlington, 1990
12. R.W. Monroe and C.E. Bates, *J. Heat Treat.,* Vol 3, 1983, p 83-99
13. J.H. Lienhard, *A Heat Transfer Textbook,* Prentice-Hall, 1987, p 389-410
14. A. Haji-Shiekh, P.B. Aswath, and F. Buckingham, "Heat Transfer in Spray Cooling," report submitted to Trinity Forging, Inc., 21 Aug 1992
15. *Annual Book of ASTM Standards,* Part 10, ASTM, 1982, p 197-293
16. C.I. Garcia, A.K. Lis, and A.J. DeArdo, *Microalloyed Bar and Forging Steels,* M. Finn, Ed., Iron and Steel Institure, 1990, p 25
17. N. Shams, *Mater. Sci. Technol.,* Vol 1, 1985, p 950
18. I. Weiss, G.L. Fitzsimmons, K. Mielityinen-Titto, and A.J. DeArdo, in *Thermomechanical Processing of Microalloyed Austenite,* A.J. DeArdo, G.A. Ratz, and P.J. Wray, Ed., AIME, 1981, p 33
19. M. Leap, E.L. Brown, P. Mazzare, and G. Krauss, in *Fundamentals of Microalloying Forging Steels,* G. Krauss and S.K. Banerji, Ed., TMS, 1987, p 91
20. P.H. Wright, T.L. Harrington, W.A. Szilva, and T.R. White, in *Fundamentals of Microalloying Forging Steels,* G. Krauss and S.K. Banerji, Ed., TMS, 1987, p 541
21. K.J. Grassl, W.A. Szilva, J.W. Weith, and P.H. Wright, private communication, Chaparral Steel Co., Midlothian, TX, 1992
22. R.W.K. Honeycombe, in *HSLA Steels—Metallurgy and Applications,* J.M. Gray et al. Eds., ASM International, 1985, p 243
23. M.L. Santella and A.J. DeArdo, in *Thermomechanical Processing of Microalloyed Austenite,* A.J. DeArdo, G.A. Ratz, and P.J. Wray, Ed., AIME, 1981, p 83
24. L.A. Touryan, S.W. Thompson, D.K. Matlock, and G. Krauss, in *Microalloyed Bar and Forging Steels,* M. Finn, Ed., Iron and Steel Institure, 1990, p 63
25. H. Nordberg and B. Aronson, *J. Iron Steel Inst.,* Vol 206, 1968, p 1263
26. L. Xiuqiu and C. Wenxuan, *HSLA Steels—Metallurgy and Applications,* J.M. Gray et al. Eds., ASM International, 1985, p 235
27. T. Gladman and F.B. Pickering, *J. Iron Steel Inst.,* Vol 205, 1967, p 653
28. A.K. Sinha, *Ferrous Physical Metallurgy,* Butterworths, 1989, p 172
29. R.W.K. Honeycombe and F.B. Pickering, *J. Iron Steel Inst.,* Vol 2, 1972, p 1099
30. A.J. DeArdo, in *Accelerated Cooling of Rolled Steel,* G.E. Ruddle and A.F. Crawley, Ed., Pergamon Press, 1987, p 3
31. L.E. Collins, R.F. Knight, G.E. Ruddle, and J.D. Boyd, in *Accelerated Cooling of Steel,* P.D. Southwick, Ed., TMS, 1985, p 261
32. I. Kozasu, in *Accelerated Cooling of Steel,* P.D. Southwick, Ed., TMS, 1985, p 15
33. M. Imagumbai and M. Nagumo, in *Accelerated Cooling of Steel,* P.D. Southwick, Ed., TMS, 1985, p 297
34. T. Tanaka, in *Accelerated Cooling of Rolled Steel,* G.E. Ruddle and A.F. Crawley, Ed., Pergamon Press, 1987, p 187
35. K.J. Irvine and F.B. Pickering, *J. Iron Steel Inst.,* Vol 201, 1963, p 518